

Temperature induced reversible structural and magnetic changes in a crystal of tetrachlorosemiquinone anion radical

Supporting Information

Krešimir Molčanov¹, Biserka Kojić-Prodić^{1*}, Darko Babić¹, Damir Pajić², Nikolina Novosel², Krešo Zadro²

¹Rudjer Bošković Institute, Bijenička c. 54, HR-10000 Zagreb, Croatia

²Department of Physics, Faculty of Science, University of Zagreb, Bijenička c. 32,
HR-10000, Zagreb, Croatia

e-mail: kojic@irb.hr

Details of experimental

S1 Preparation, crystallization and crystallographic data

S2 Magnetic susceptibility

S3 Computational details

S4 References

S1 Preparation of samples and X-ray structure analysis

Potassium and ammonium salts of tetrachlorosemiquinone anion radical were obtained according to the literature (Torrey & Hunter, 1912; Molčanov *et al*, 2011) and crystallized from 2-butanone and acetonitrile. Crystals appropriate for X-ray structure analysis were obtained in fifteen minutes but in solution they decomposed in less than an hour. Thermogravimetric and differential thermal analysis reveal loss of solvent in the range 315 – 338 K followed by a collapse of the crystal structure as confirmed by a lack of diffraction pattern. However, the radical remains stable up to 370 K.

The short lifetime of samples in air (2 – 3 min) was just enough to select single crystals under a stereomicroscope, glue them to a glass needle and mount into a stream of cold nitrogen gas. Intensity data collections for the two polymorphs were measured at 100 and 200 K on an Oxford Diffraction Xcalibur Nova R diffractometer (microfocus Cu-tube, CCD detector) equipped with an Oxford Instruments Cryojet liquid nitrogen cooling device. Crystallographic data and details on data collection, and structure refinement are provided in the Table 1.

Program package CrysAlis PRO (CrysAlis, 2007)³⁶ was used for data reduction. The structures were solved using SHELXS97 (Sheldrick, 2008)³⁷ and refined with SHELXL97 (Sheldrick, 2008)³⁷. The models were refined using the full-matrix least squares refinement; all non-hydrogen atoms were refined anisotropically. Hydrogen atoms were located in a difference Fourier map and refined using the following restraints: $d(\text{O}_{\text{hydroxyl}}-\text{H}) = 0.82 \text{ \AA}$, $d(\text{O}_{\text{water}}-\text{H}) = 0.95 \text{ \AA}$; $d(\text{H}-\text{H}) = 1.50 \text{ \AA}$. Molecular geometry calculations were performed by PLATON (Spek, 2003)³⁸, and molecular graphics were prepared using ORTEP-3 (Farrugia, 1997)³⁹. Supplementary crystallographic data for this paper can be obtained free of charge *via* www.ccdc.cam.ac.uk/conts/retrieving.html (or from the Cambridge Crystallographic Data Centre, 12, Union Road, Cambridge CB2 1EZ, UK; fax: +44 1223 336033; or deposit@ccdc.cam.ac.uk). CCDC-849635, 849636 & 855438 contain the supplementary crystallographic data for this paper.

The gradual and reversible single crystal-to-single crystal phase transition of $\text{KCl}_4\text{Q}\cdot\text{MeCOEt}$ was monitored by measuring the unit cell parameters in the range 120 – 170 K, with a step of 5 K; the volume of monoclinic unit cell ($P2_1/c$) of HT-polymorph was reduced by a half comparing to the volume of LT-polymorph (Table 1 and Figures 2- overlap of unit cells, and S6). The structural change during the phase transition involves the

rearrangement of radical anion stacks from dimers to monomers. The quantitative measures of this change are the interradical anion separation distance.

The anion radical in both polymorphs of $\text{KCl}_4\text{Q}^\cdot\text{-MeCOEt}$ has no molecular symmetry, while in $\text{NH}_4\text{Cl}_4\text{Q}^\cdot\text{-MeCN}$ its centroid is located in an inversion center, therefore its symmetry is C_i . However, an approximate molecular D_{2h} symmetry can be considered. The tetrachlorosemiquinone anion radical reveals greater aromaticity in comparison to quinone as assessed by the nucleus independent chemical shift analysis (NICS).

The local environment of one potassium cation (K^+) in the LT-polymorph is of similar geometry to the one in the HT-polymorph: six neighbouring atoms including five oxygen atoms of anion and solvent and one chlorine (Figs. S3 and S4 & Table S2). However, the local environment of the other cation (K^+) in the LT-polymorph is different to that one of the K^+ (and also one in HT-polymorph). It exhibits seven coordination including the two chlorine atoms with distances $\text{K}^+\cdots\text{Cl}$ of 3.417 (1) and 3.450 (1) Å.

Table S1 Bond lengths in tetrachlorosemiquinone radical anions.

	KCl ₄ Q [·] -MeCOEt			NH ₄ Cl ₄ Q [·] -MeCN
	100 K (molecule A)	100 K (molecule B)	200 K	100 K
C1 – C2	1.448(5)	1.450(5)	1.449(4)	1.448(5)
C2 – C3	1.362(5)	1.366(5)	1.365(4)	1.369(5)
C3 – C4	1.447(6)	1.463(6)	1.445(4)	1.448(5)*
C4 – C5	1.451(5)	1.444(5)	1.446(4)	1.452(5)*
C5 – C6	1.366(5)	1.369(5)	1.371(4)	1.369(5)*
C6 – C1	1.448(6)	1.451(6)	1.442(4)	1.452(5)
C1 – O1	1.253(4)	1.251(4)	1.253(3)	1.260(5)
C4 – O2	1.254(4)	1.258(4)	1.252(3)	1.260(5)*
C2 – Cl1	1.722(4)	1.722(4)	1.718(3)	1.722(4)
C3 – Cl2	1.726(4)	1.721(4)	1.730(3)	1.720(4)
C5 – Cl3	1.726(4)	1.722(4)	1.721(3)	1.722(4)*
C6 – Cl4	1.724(4)	1.723(4)	1.728(3)	1.720(4)*

*Symmetry equivalent.

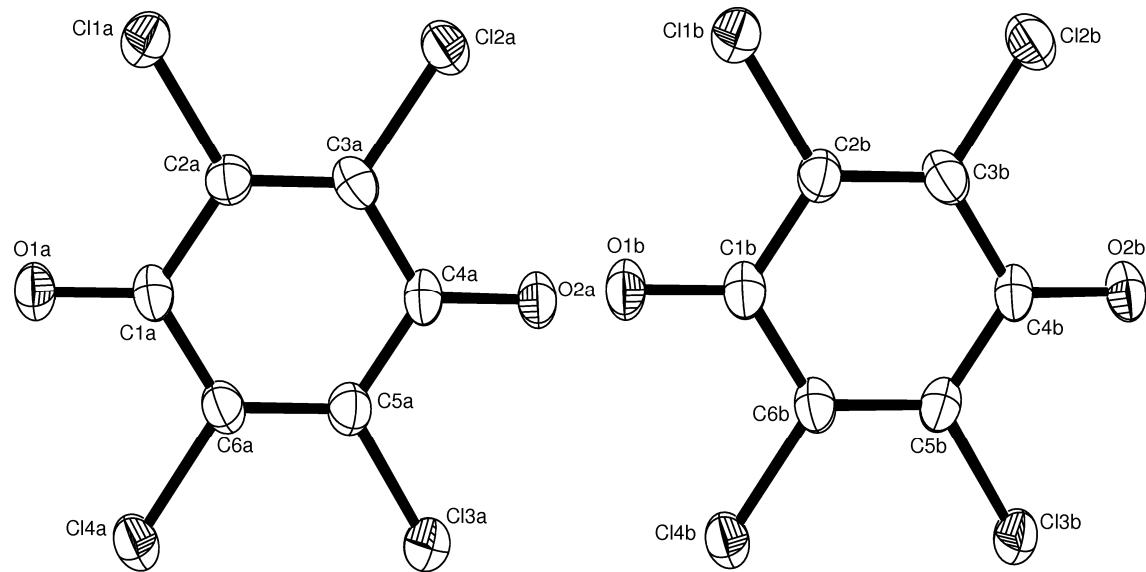


Figure S1 ORTEP-3 drawings of two symmetry-independent tetrachlorosemiquinone radical anions (A and B) in LT KCl₄Q[•]·MeCOEt. Displacement ellipsoids are drawn at the probability of 50 %.

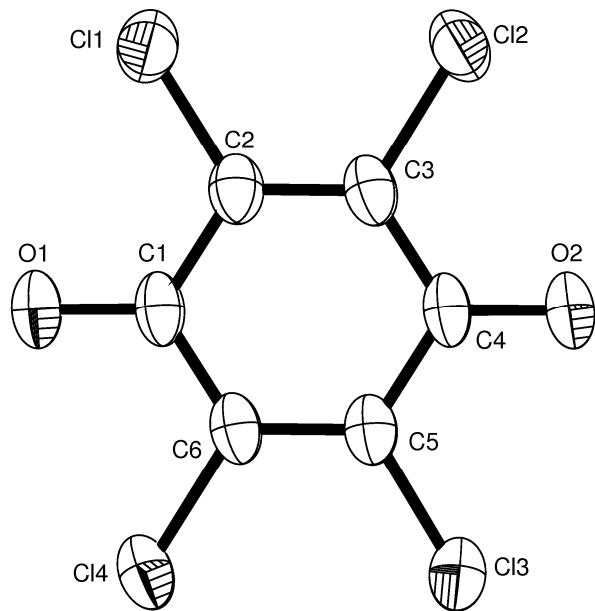


Figure S2 ORTEP-3 drawing of tetrachlorosemiquinone radical anions in HT KCl₄Q[•]·MeCOEt. Displacement ellipsoids are drawn at the probability of 50 %.

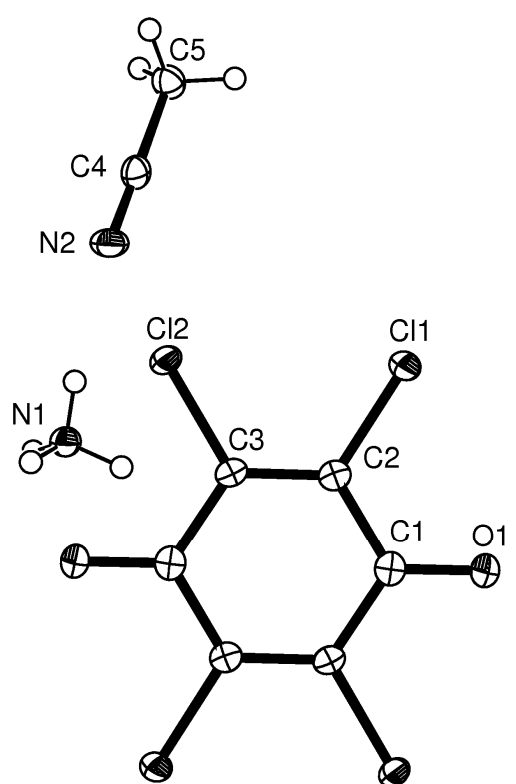


Figure S3 ORTEP-3 drawing of asymmetric unit of $\text{NH}_4\text{Cl}_4\text{Q}^\bullet\text{-MeCN}$. Displacement ellipsoids are drawn at the probability of 50 %.

Table S2 Geometry of potassium cation coordination sphere in LT (100 K) and HT (200 K) structure of $\text{KCl}_4\text{Q}^\bullet\cdot\text{MeCOEt}$ (\AA , $^\circ$).

	100 K (molecule A)	100 K (molecule B)		200 K	
K1 – O1A	2.643 (3)	K2 – O2B ⁱⁱ	2.681 (3)	K1 – O1 ^{iv}	2.671(2)
K1 – O3 (solvent)	2.648 (4)	K2 – O2A ⁱⁱ	2.684 (3)	K1 – O1 ^v	2.672(2)
K1 – O1B	2.656 (3)	K2 – O1B	2.688 (3)	K1 – O3 (solvent)	2.675(3)
K1 – O2A ⁱ	2.705 (3)	K2 – O1A ⁱⁱⁱ	2.695 (3)	K1 – O2	2.703(2)
K1 – O2B ⁱⁱ	2.795 (3)	K2 – O4 (solvent)	2.695 (4)	K1 – O2 ^{vi}	2.739(2)
K1 – Cl2B ⁱⁱ	3.293 (1)	K2 – Cl1B	3.417 (1)	K1 – Cl2 ^{vi}	3.383(1)
O1A – K1 – O3	106.2 (1)	K2 – Cl2A ⁱⁱ	3.450 (1)	O1 ^{iv} – K1 – O1 ^v	98.80(7)
O1A – K1 – O1B	86.0 (1)	O2B ⁱⁱ – K2 – O2A ⁱⁱ	85.27 (9)	O1 ^{iv} – K1 – O3	108.60(8)
O1A – K1 – O2A ⁱ	78.68 (9)	O2B ⁱⁱ – K2 – O1B	82.83 (9)	O1 ^{iv} – K1 – O2	78.84(7)
O1A – K1 – O2B ⁱⁱ	160.4 (1)	O2B ⁱⁱ – K2 – O1A ⁱⁱⁱ	161.0 (1)	O1 ^{iv} – K1 – O2 ^{vi}	159.03(7)
O1A – K1 – Cl2B ⁱⁱ	106.47 (7)	O2B ⁱⁱ – K2 – O4	105.3 (1)	O1 ^{iv} – K1 – Cl2 ^{vi}	103.35(5)
O3 – K1 – O1B	94.2 (1)	O2B ⁱⁱ – K2 – O3	124.51 (7)	O1 ^v – K1 – O3	90.30(8)
O3 – K1 – O2A ⁱ	117.2 (1)	O2B ⁱⁱ – K2 – Cl2A ⁱⁱ	74.47 (7)	O1 ^v – K1 – O2	158.85(7)
O3 – K1 – O2B ⁱⁱ	89.7 (1)	O2A ⁱⁱ – K2 – O1B	153.6 (1)	O1 ^v – K1 – O2 ^{vi}	78.19(7)
O3 – K1 – Cl2B ⁱⁱ	146.36 (9)	O2A ⁱⁱ – K2 – O1A ⁱⁱⁱ	78.15 (9)	O1 ^v – K1 – Cl2 ^{vi}	84.70(5)
O1B – K1 – O2A ⁱ	147.8 (1)	O2A ⁱⁱ – K2 – O4	94.5 (1)	O3 – K1 – O2	110.46(8)
O1B – K1 – O2B ⁱⁱ	81.29 (9)	O2A ⁱⁱ – K2 – Cl1B	147.04 (7)	O3 – K1 – O2 ^{vi}	92.24(8)
O1B – K1 – Cl2B ⁱⁱ	80.35 (7)	O2A ⁱⁱ – K2 – Cl2A ⁱⁱ	55.18 (7)	O3 – K1 – Cl2 ^{vi}	148.05(7)
O2A ⁱ – K1 – O2B ⁱⁱ	104.59 (9)	O1B – K2 – O1A ⁱⁱⁱ	108.29 (9)	O2 – K1 – O2 ^{vi}	96.43(7)
O2A ⁱ – K1 – Cl2B ⁱⁱ	77.15 (7)	O1B – K2 – O4	111.4 (1)	O2 – K1 – Cl2 ^{vi}	75.55(5)
O2B ⁱⁱ – K1 – Cl2B ⁱⁱ	56.72 (7)	O1B – K2 – Cl1B	55.53 (7)	O2 ^{vi} – K1 – Cl2 ^{vi}	55.84(5)
		O1B – K2 – Cl2A ⁱⁱ	98.83 (7)		
		O1A ⁱⁱⁱ – K2 – O4	85.3 (1)		
		O1A ⁱⁱⁱ – K2 – Cl1B	74.01 (7)		
		O1A ⁱⁱⁱ – K2 – Cl2A ⁱⁱ	88.38 (7)		
		O4 – K2 – Cl1B	66.22 (8)		
		O4 – K2 – Cl2A ⁱⁱ	149.63 (9)		
		Cl1B – K2 – Cl2A ⁱⁱ	139.56 (4)		

i) $-x, 1/2+y, 1/2-z$; *ii)* $1-x, 1/2+y, 1/2-z$; *iii)* $1+x, y, z$; *iv)* $-x, -1/2+y, 1/2-z$; *v)* $-1-x, -1/2+y, 1/2-z$; *vi)* $-1+x, y, z$.

Table S3 Geometric parameters of hydrogen bonds in $\text{NH}_4\text{Cl}_4\text{Q}^\bullet\cdot\text{MeCN}$.

	D–H / Å	H···A / Å	D···A / Å	D–H···A / °	Symm. op. on A
N1–H1A···O1	0.87(3)	1.94(4)	2.754(4)	154(3)	$1-x, 1-y, 1-z$
N1–H1B···N2	0.86(2)	2.05(2)	2.901(6)	170(6)	x, y, z
C5–H5B···O1	0.95(4)	2.52(5)	3.282(5)	137(4)	$1-x, 1-y, -z$

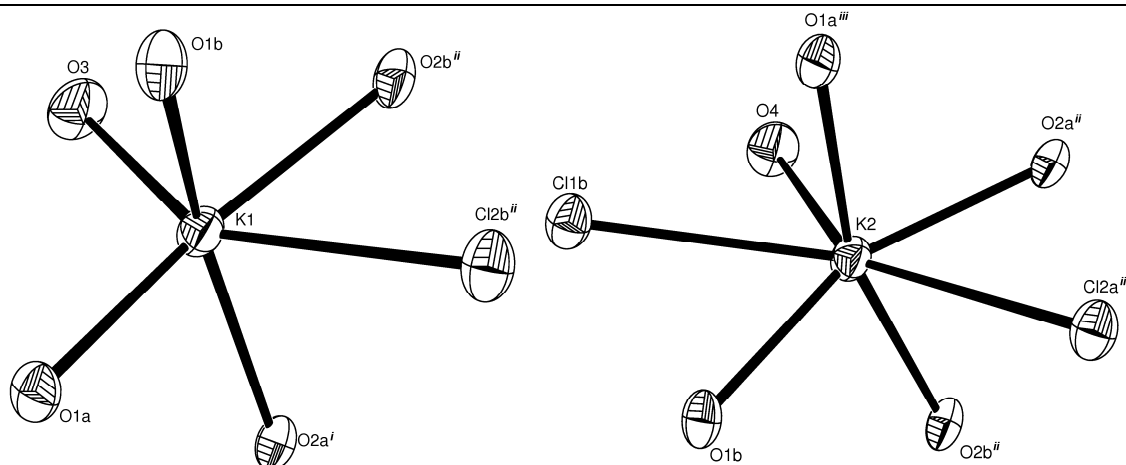


Figure S4 ORTEP-3 drawings of coordination spheres of potassium cations in LT $\text{KCl}_4\text{Q}^\bullet\cdot\text{MeCOEt}$. Displacement ellipsoids are drawn at the probability of 50 %. Symmetry operators are given at the bottom of Table S3. Potassium cation K^{+} is surrounded by six neighbors, whereas the seventh closest one is Cl^{4A} ($-x, -1/2+y, 1/2-z$) at the distance 3.591(4) Å (not plotted). The cation K^{+} reveals seven neighbors with the two chlorine atoms at distances of 3.417 (1) and 3.450(1) Å.

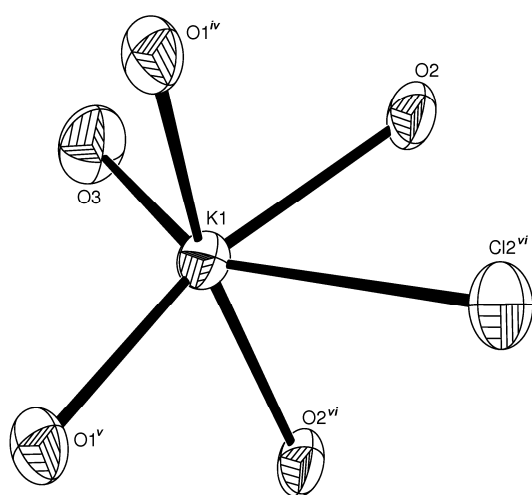


Figure S5 ORTEP-3 drawings of coordination sphere of potassium cation in HT KCl₄Q[•]·MeCOEt. Displacement ellipsoids are drawn at the probability of 50 %. Symmetry operators are given at the bottom of Table S3. The seventh closest neighbor is Cl1 ($-x$, $-1/2+y$, $1/2-z$) of 3.596(1) Å (not plotted).

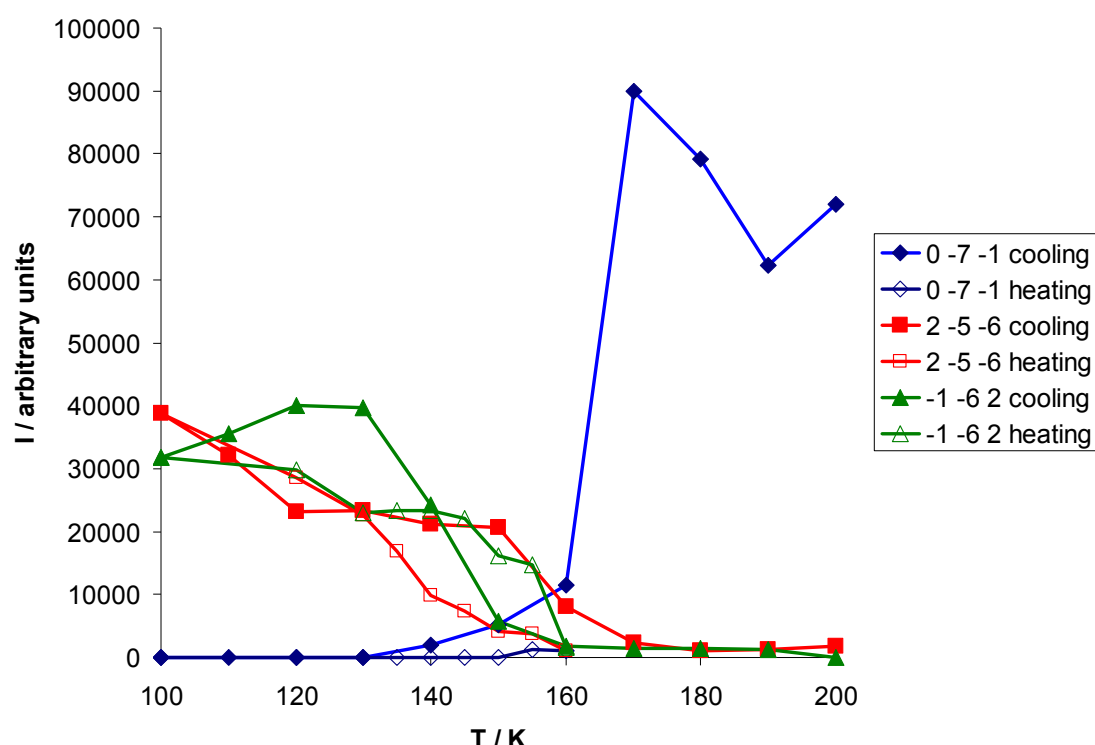


Figure S6 Diffraction intensities continuously change with temperature when cooling (full symbols) and heating (empty symbols), indicating a continuous phase transition. Two reflections of low-temperature phase [$(2\bar{5}\bar{6})$, in red, and $(\bar{1}\bar{6}2)$, in green] and one reflection of high-temperature phase [$(0\bar{7}\bar{1})$, in blue] are shown. In the temperature interval 140 - 160 K reflections of both phases are observed, and both unit cells can be indexed. All data were measured with the same single-crystal; raw diffraction intensities (no data reduction) are used for the plot presented.

S2 Magnetic susceptibility

Magnetic properties of $\text{KCl}_4\text{Q}^\bullet\text{-MeCOEt}$ and $\text{NH}_4\text{Cl}_4\text{Q}^\bullet\text{-MeCN}$ were investigated using MPMS-5 SQUID magnetometer. 100 mg of powder was measured in ampoule whose diamagnetic contribution was subtracted properly. Temperature dependence of magnetization $M(T)$ was measured in several applied magnetic fields in a broad temperature range (5 – 370 K). Magnetization versus field $M(H)$ was measured at several characteristic temperatures in field range of –5 T to 5 T.

Prior to quantitative analysis of the magnetic transition, the correction of data against the paramagnetic contribution, observable as the increase of susceptibility at the lowest temperatures, has been performed. The data for $T < 50$ K were fitted with Curie's law with added diamagnetic term χ_0

$$\chi_{corr.}(T) = \chi_0 + \rho \frac{N_A \mu_B^2 g^2}{4 k_B T}$$

where ρ is amount of paramagnetic impurities of spin $S = 1/2$. Taking $g = 2$, the fitting resulted with $\chi_0 = -132 \cdot 10^{-6}$ emu/mol and $\rho = 0.0049$. Obtained $\chi_{corr.}$ was subtracted from all the data and presented in Figure S7.

Having in mind the dimerization in LT structure, modeling of magnetic measurements using the notion of magnetic dimers is performed. The structure starts to change above 120 K, therefore the magnetic units below 120 K could be assumed as fixed and the Bleaney-Bowers [Bleaney, B., Bowers, K.D. Proc. Royal Soc. London A **214**, 451–465 (1952)] model of antiferromagnetically coupled spin pairs was used. Fitting of susceptibility per mole of formula units (half of dimers) was done using the equation:

$$\chi_{BB} = \frac{N_A \mu_B^2 g^2}{k_B T \left(3 + \exp(-J_{dim}/T) \right)}$$

where J_{dim} is exchange coupling defined within isotropic Heisenberg interaction $H = -J_{dim}S_1S_2$, and the value $J_{dim} = -640(10)$ K is obtained. Above the temperature of 120 K the value of measured susceptibility is above the dimeric model value (Figure S7), that is accompanied to the change/increase of distance between the units in dimer. Therefore, the region above 120 K can not be treated in this way.

Periodic HT structure is featured with considerably lower susceptibility and different trend than in simple paramagnetic case. Therefore, the chain with antiferromagnetic coupling between neighboring units is assumed as a model of magnetic properties, and Bonner-Fisher [Bonner, J.C., Fisher, M.E., *Phys. Rev.* **135**, A640 (1964)] expression

$$\chi_{BF} = \frac{N_A \mu_B^2 g^2}{k_B T} \cdot \frac{0.25 + 0.074975 y + 0.075235 y^2}{1 + 0.9931 y + 0.172135 y^2 + 0.757825 y^3}$$

is used, where $y = |J_{chain}|/T$, with $J_{chain} < 0$ being the isotropic antiferromagnetic exchange parameter defined in Heisenberg spin chain model Hamiltonian $H = -J_{chain} \sum S_i S_{i+1}$. This expression fitted to the data for $T > 190$ K, where the structure does not change any more, gives $J_{chain} = -260(10)$ K.

We performed the iterative fitting of both HT and LT region of magnetic data, in order to settle with better accuracy into fitting parameter space. Such relatively large deviations/errors of parameters are caused with extrapolation of both models: Bonner-Fisher to HT region only and Bleaney-Bowers to LT region only. The inclusion of interaction between the chains was tried without success in describing the data and resulting with unphysical parameters.

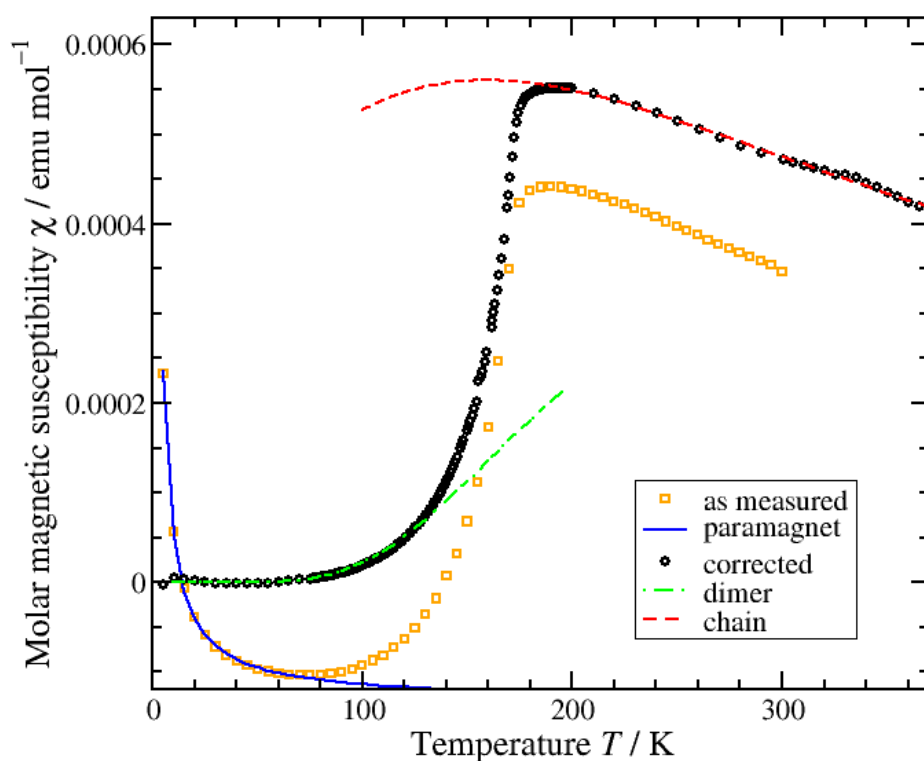


Figure S7 Temperature dependence of molar magnetic susceptibility χ of $\text{KCl}_4\text{Q}^\bullet\text{-MeCOEt}$ measured in the field of 1T. Squares represent the measured data, continuous line the Curie's fit, circles the data corrected against the Curie's and diamagnetic background terms, dash-dot line the LT dimer model and dashed line the HT spin chain model.

Magnetization versus field $M(H)$ was measured at several characteristic temperatures in field range of -5 T to 5 T (Figure S8). The linearity of $M(H)$ was checked in LT and HT phase, as well as in the temperature range where the structural change happens. Therefore, it is justified to use the magnetic susceptibility as the proper physical quantity for analysis.

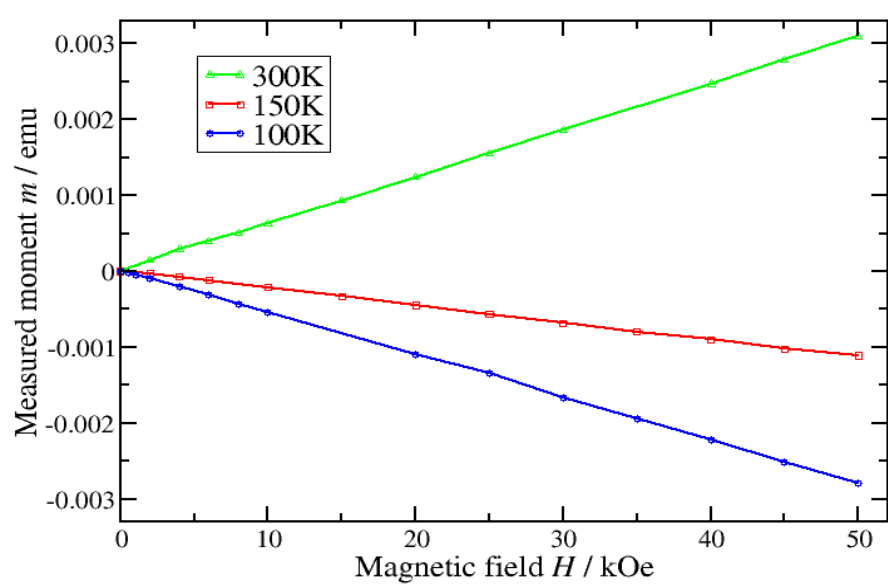


Figure S8 Field dependence of magnetic moment of $\text{KCl}_4\text{Q}\cdot\text{MeCOEt}$ measured at different temperatures.

S3 Computational details

Table S4. Computational results of the electronic structure of the KCl₄Q pairs taken out from the crystal structures at low (**LT-S** and **LT-L**) and high (**HT**) temperatures

	s/t ^{a)}	LT-S	LT-L	HT
E(CAS) / H	s	-5628.506549	-5628.513053	-5628.512621
	t	-5628.503606	-5628.513080	-5628.512310
Δ E(CAS) / kJ/mol	s-t	-7.727	0.071	-0.817
E(UMP2) / H	s	-5633.817017	-5633.809158	-5633.811579
	t	-5633.813832	-5633.809187	-5633.811289
Δ E(UMP2) / kJ/mol	s-t	-8.362	0.076	-0.761
MCSCF (CAS) coeffs. ^{b)}	s	+0.808393	+0.719443	+0.746211
		+0.0000002	+0.0000001	-0.0000002
		-0.588643	-0.694552	-0.6657091
		+0.999995	+0.999994	+0.999993
		+0.002659	-0.003270	-0.003534
	t	+0.001591	+0.001398	+0.001169
		-0.111479	+0.012499	-0.040541
		+0.987851	+0.999845	+0.998378
		-0.108271	+0.012392	-0.039961
		+0.999995	+0.999994	+0.999993
MCSCF (CAS) coeffs. ^{b)} after Boys localization	s	+0.002659	-0.003270	-0.003534
		+0.001591	+0.001398	+0.001169
	t	1.00	1.00	1.00
		1.00	1.00	1.00
		1.00	1.00	1.00
occ. nos. after Boys localization ^{c)}	s	1.00	1.00	1.00
		1.00	1.00	1.00
	t	0.00	0.00	0.00
		1.00	1.00	1.00
		1.00	1.00	1.00
E(wB97XD) / H	s	-5639.803432	-5639.804222	-5639.804779
	t	-5639.802012	-5639.804209	-5639.804609
Δ E(wB97XD) / kJ/mol	s-t	-3.728	-0.034	-0.446
<S ² > (<S> ^{d)}	s	1.01 (0.62)	1.04 (0.64)	1.04 (0.64)
	t	2.03 (1.01)	2.03 (1.01)	2.03 (1.01)

a) **s** = singlet state, **t** = triplet state, **s-t** = singlet – triplet difference

- b) from top to bottom, the numbers for the singlet states refer to the active space configurations $(\alpha\beta,00)$, $(\alpha0,\beta0)$ and $(00,\alpha\beta)$, respectively, and for the triplet states to configurations $(\alpha0,\alpha0,00)$, $(\alpha0,00,\alpha0)$ and $(00,\alpha0,\alpha0)$, respectively
- c) occupation numbers refer to HOMO and LUMO orbitals for the singlet state, and to the HOMO, LUMO and LUMO+1 orbitals, from top to bottom, for the triplet state
- d) $\langle S^2 \rangle$ stands for estimate of the squared spin angular momentum and $\langle S \rangle$ for the expected S on the basis of the formula $S^2 = S(S+1)$.